Ore Geology Reviews 102 (2018) 894–905

Contents lists available at ScienceDirect

Ore Geology Reviews

journal homepage: www.elsevier.com/locate/oregeorev

Tellurium, magmatic fluids and orogenic gold: An early magmatic fluid pulse at Cononish gold deposit, Scotland

Carl P. Spence-Jones[a,*], Gawen R.T. Jenkin[b], Adrian J. Boyce[c], Nyree J. Hill[b,d], Christopher J.S. Sangster[d]

[a] School of Earth and Environment, University of Leeds, Leeds LS2 9JT, United Kingdom
[b] School of Geography, Geology and the Environment, University of Leicester, Leicester LE1 7RH, United Kingdom
[c] Scottish Universities Environmental Research Centre, Rankine Avenue, Scottish Enterprise Technology Park, East Kilbride G75 0QF, United Kingdom
[d] Scotgold Resources, Upper Station, Tyndrum, Stirlingshire FK20 8RY, United Kingdom

ARTICLE INFO

Keywords:
Neoproterozoic
Orogenic gold
Magmatic fluid
Gold
Tellurium
Silver

ABSTRACT

Significant tellurium enrichment occurs in many orogenic gold deposits but the factors causing this are little understood; some authors suggest this demands a magmatic input whereas others suggest it need not. Fractionation of Te from Se and S could offer insight into source/pathway processes of auriferous fluids. The metasedimentary-hosted Cononish vein gold deposit, Scotland, is unusually Te-rich compared to many orogenic gold deposits with Te/Au ≈ 2.4 whereas most orogenic deposits have Te/Au < 1. Here, Ag in Au-Ag alloy increases from ~10 to 90 wt% through the paragenesis, correlating with decreasing hessite (Ag_2Te) abundance. This suggests the Au-Ag alloy composition was controlled by the fluid Te activity, and that this decreased through time. This is coupled to an increase in pyrite $\delta^{34}S$ from −2.0‰ to +11.4‰ through the paragenesis. Thus, the deposit formed from a primary fluid with a low-$\delta^{34}S$ and high Te + Au + Ag that evolved to a high $\delta^{34}S$-low Te, Pb + Cu bearing fluid. The high $\delta^{34}S$ of the later fluid suggests it can only be sourced from specific nearby metamorphosed SEDEX horizons. The early fluid that deposited most of the gold could be sourced from other metasedimentary units in the stratigraphy or be magmatic in origin. We argue that two observations taken together suggest it is most likely that this fluid was magmatic; the age of the mineralisation is identical to the last stage of crystallization of nearby granite batholiths, and the fluid has a S-isotope signature consistent with a magmatic source. Gold deposits in orogenic belts are almost certainly polygenetic and this study demonstrates evidence for Te-rich "orogenic" deposits having a significant magmatic component.

1. Introduction

Orogenic gold deposits formed in metamorphic terranes are a broad class of deposits exhibiting a common set of features (Goldfarb et al., 2005) and are typically deposited from low-salinity CO_2-bearing fluids (Goldfarb and Groves, 2015). Despite commonality of broad features, variations in isotopic composition, mineral assemblage, and metal enrichments exist (Chapman and Mortensen, 2016; Goldfarb and Groves, 2015; Groves et al., 1998), and the interpreted source of the ore fluids, and the dissolved constituents they transport, remains controversial (Goldfarb et al., 2005; Goldfarb and Groves, 2015; Wyman et al., 2016). Whilst a metamorphic fluid source from devolatilisation of metasedimentary or metabasic rocks remains the most likely model for the majority of orogenic deposits (Goldfarb et al., 1993; Pettke et al., 1999; Large et al., 2009; Phillips and Powell, 2010; Pitcairn et al., 2014; Pitcairn et al., 2015), input of magmatic or mantle-derived fluids has been invoked to explain variations in metal enrichments, isotopic compositions and mineralogical distinctions of individual orogenic gold deposits (Kerrich, 1989; Kerrich and Wyman, 1990; Sillitoe and Thompson, 1998; Robert 2001; Goldfarb et al., 2005; Yoo et al., 2010; Hammond et al., 2011; McFarlane et al., 2011; Treloar et al., 2015). The latter do not include the more clearly recognised sub-group of reduced intrusion-related gold deposits in which magmatic fluid input is generally acknowledged (Hart and Goldfarb, 2005; Goldfarb et al., 2005). The cause of the common Te-enrichment in orogenic gold deposits (Goldfarb et al., 2016) mirrors this dichotomy, with some workers advocating that enrichment indicates a magmatic source (Burrows and Spooner, 1989) whereas others suggest it need not (Goldfarb et al., 2000; 2016). Understanding the controls on Te enrichment in orogenic systems is topical given the increasing interest in this element for use in solar photovoltaic technology (Woodhouse et al., 2013; Goldfarb et al., 2016). Whilst all orogenic gold deposits show

* Corresponding author.
E-mail address: C.Spence-Jones@leeds.ac.uk (C.P. Spence-Jones).

https://doi.org/10.1016/j.oregeorev.2018.05.014
Received 9 January 2018; Received in revised form 14 May 2018; Accepted 20 May 2018
Available online 25 May 2018

some enrichment in Te compared to bulk continental crust (~5 ppb; Wedepohl, 1995), there is a considerable range in the enrichments. Some lower values of Te are associated with deposits that have no connection with magmatic activity (e.g. deposits in the Otago and Alpine Schist, New Zealand; Pitcairn et al., 2006). So, conversely, it is possible that some examples of Te-enrichment in orogenic deposits (Goldfarb et al., 2016) result from magmatic input, as is almost certainly the case in many of the better recognized group of reduced intrusion-related gold deposits in orogenic belts (Thompson et al., 1999). The alternative is that Te enrichment is unrelated to magmatic input but simply a result of a particular combination of source, transport and precipitation processes operating in orogenic gold systems.

The planned development of the Cononish gold mine in the Scottish Highlands (estimated reserves of 555,000 tonnes of ore grading at 11.1 g/t Au and 47.7 g/t Ag; Scotgold Resources Limited, 2015), alongside the development of Curraghinalt and Cavanacaw mines in Ireland, has catalysed a re-evaluation of gold metallogenesis in the Caledonides. The Cononish deposit is structurally-controlled in a splay off a major fault, is hosted in lower-amphibolite facies rocks and formed late in the deformation history of the host orogen – thus it conforms to many of the features that define orogenic gold deposits *sensu* Groves et al. (2003), it is classed as orogenic by the review of Goldfarb et al. (2005) and this view persists with some observers (Goldfarb pers. comm. 2013). The deposit notably contains significant Te – the Te/Au ratio by weight of ore grade material is ≥ 1, suggesting > 7 t Te (Science and Technology Committee, House of Commons, 2011). Cononish is Te-rich compared to most orogenic gold deposits (including those identified as intrusion-related) and shows enrichment of Te compared to Se along a trend comparable to the overall trend observed for orogenic gold deposits, with high Au grade Cononish samples reaching the extremes of this trend (Fig. 1A). Cononish also shows high Te/Au – approximately 75% of data from orogenic gold deposits have Te/Au < 1, whereas at Cononish average Te/Au is 2.4 and only 17% of data have Te/Au < 1 (Fig. 1B). Thus, Cononish represents a Te-rich gold system in an orogenic belt which may provide insight on the causes of Te-enrichment and the deposit provides an excellent system in which to study the fluids and processes that formed the mineralisation. Approximately 2 km of unlined exploration adits along with well curated exploration and development data from drill programs are accessible. Fluid inclusion and stable isotope data are available, along with textural and mineralogical descriptions of the mineralised veins (Pattrick et al., 1988; Earls et al., 1992; Curtis et al., 1993). However, the detailed paragenesis of the veins has never been described and linked to mineral chemistry and stable isotope data. Furthermore, the genesis of the deposit remains contentious, with either magmatic or metamorphic fluids (± meteoric) interpreted to have formed the deposit (Pattrick et al., 1988; Curtis et al., 1993; Craw and Chamberlain, 1996). Here, a combined study of the paragenesis, Au-Ag alloy composition, and sulfur isotope ratios provides evidence for an early Te-bearing magmatic fluid, with potential implications for the genesis of other orogenic deposits with high Te/Au.

2. Geological setting

The Cononish deposit is in the Tyndrum area, approximately 70 km north of Glasgow, Scotland. The area comprises Neoproterozoic Dalradian Supergroup metasediments that were subjected to amphibolite-grade metamorphism and deformation (D_1–D_4) during the Grampian Orogeny, ~470 Ma (Stephenson et al., 2013). The sequence is dissected by major NE-trending sinistral faults with a normal component that developed late in the orogeny, including the Tyndrum fault. The Cononish deposit, located 3 km south west of Tyndrum, comprises a composite vein structure hosted within the sub-vertical Cononish Fault (041/89SE), formerly known as the Eas Anie Fault. The Cononish Fault has a sinistral sense of displacement (Treagus et al., 1999; Tanner, 2012) and is associated with a splay off the Tyndrum Fault (see geological map in Hill et al., 2013).

The Cononish Fault crosscuts Grampian and lower-Appin Group units that were deformed into large north-east verging nappe structures during the Grampian orogeny (Tanner and Thomas, 2010; Tanner, 2012). The Cononish deposit is situated on the upper limb of the southerly dipping synformal Beinn Chuirn anticline. The stratigraphy on the lower limb of the fold is overturned and inferred to exist at depth below the deposit (Earls et al., 1992; Stephenson et al., 2013; Tanner, 2014).

Two temporally distinct vein arrays exist in the Cononish Fault and have been sampled in this study (Fig. 2). The early Cononish vein comprises Au-Ag (± Cu, Pb) mineralisation, termed "A-min" by Earls et al. (1992) and dated by Rice et al. (2012) at 408 ± 2 Ma and 407 ± 1 Ma using Ar/Ar of K-feldspar. This early Au-Ag (± Cu, Pb) mineralisation is cross-cut by a later Pb-Zn bearing quartz vein (Earls et al., 1992; Pattrick et al., 1988). This later vein was termed "B-Min" by Earls et al. (1992) and is predominantly vuggy quartz with galena and sphalerite. The open texture in the later "B" vein is in contrast to the closed crystalline texture of the early "A" vein and thus the two veins are treated as belonging to two separate fluid events in the literature (Curtis et al., 1993; Earls et al., 1992) and in this study. A Permo-Carboniferous basalt dyke clearly cuts the gold-bearing mineralisation in the adit. The relationship of the dyke to the later Pb-Zn mineralisation is more cryptic – in the surrounding area Treagus et al. (1999) state that the dykes cross-cut the Pb-Zn phase, although in the adit *some* late veining also cuts the dyke.

3. Methodology

Sampling was undertaken at Cononish with the assistance of Scotgold Resources Ltd. Samples of the veins and the host lithologies proximal to the mineralisation were collected from the 400 mL level adit (Fig. 2). Sample locations were selected based on company underground face mapping and assay data, with particular care taken to sample the range of vein textures displayed within the adit. Bulk samples taken underground were subsampled and selected hand specimens were cut and polished into slabs to reveal textures. These were then sectioned to produce 16 polished thin sections and 18 polished blocks, representing the complete range of vein textures and mineralogy. Samples were generally high grade (> 10 ppm < 160 ppm Au) with Te/Au averaging ~1.5.

Carbon-coated polished thin sections were examined using a Hitachi S-3600 N Scanning Electron Microscope operated under high vacuum (< 1 Pa) with an accelerating voltage of 15 kV in backscattered electron imaging mode. Spot chemical analyses were made using an Oxford Instruments INCA 360 energy dispersive X-ray (EDX) system. The EDX system operates with an accuracy of typically better than ± 10% relative for elemental/oxide concentrations > 10 wt% in the sample material. Precision and accuracy deteriorate as measured concentrations drop to the minimum detection limit (around the 1% level for most elements under the analytical conditions used).

For sulfur isotope analysis 16 paragenetically-constrained pyrite grains were drilled to produce powdered samples for analysis. The first 5 samples were published by Hill et al. (2013) but paragenetic assignment of the exact material sampled has been revised here. To confirm results an additional 11 constrained pyrite samples were subsequently prepared at the University of Leeds in 2015. All samples were analysed at SUERC. SO_2 was produced from sulfides by combustion with cuprous oxide for mass spectrometric analysis (Robinson and Kusakabe, 1975). Mass spectrometry was undertaken with a VG SIRA II gas mass spectrometer. Reproducibility, based on repeat analyses of internal and international lab standards (CP1, NBS 123 & IAEA S 3), was better than ± 0.3‰. All data are reported as $\delta^{34}S$ per mil (‰) relative to the Canyon Diablo Troilite standard (V-CDT).

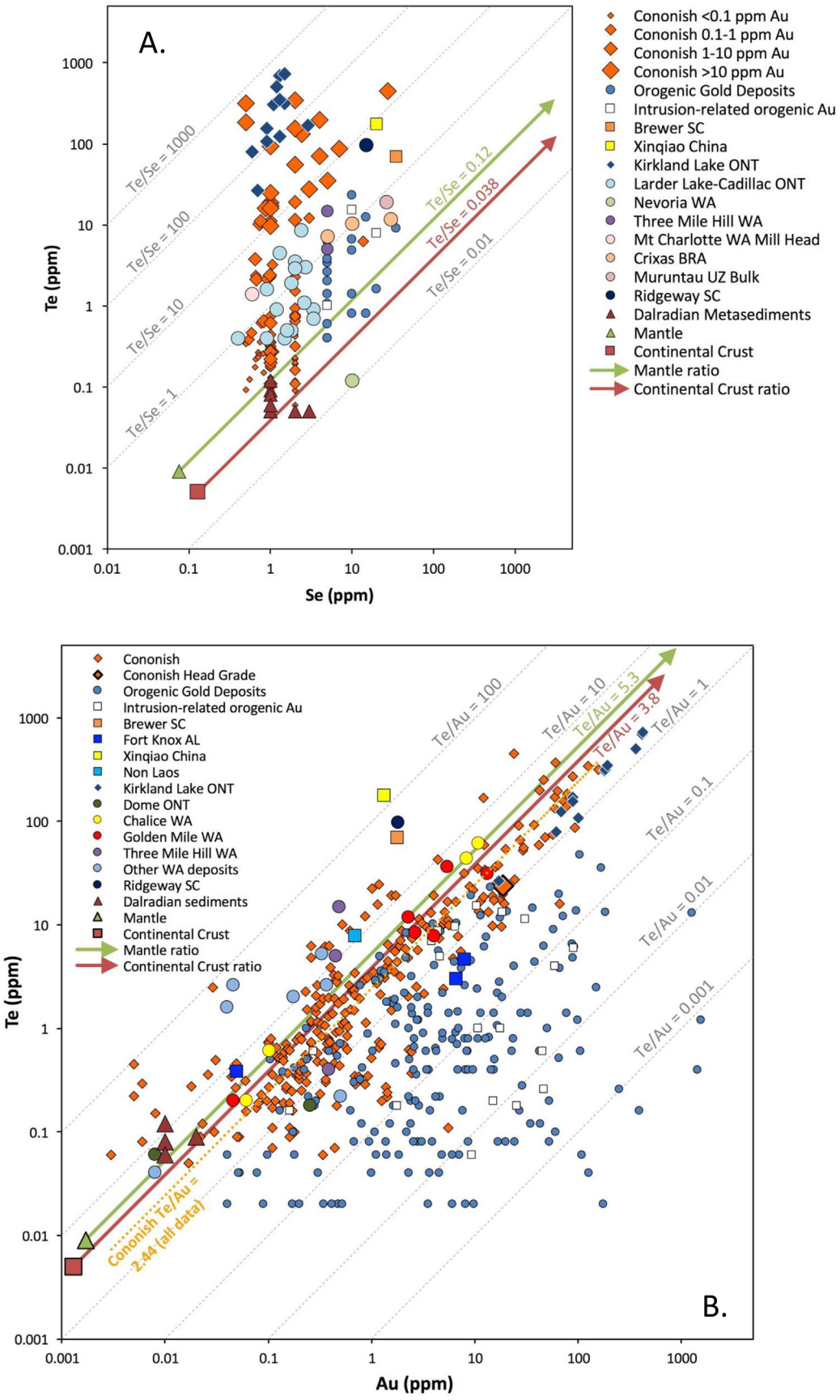

Fig. 1. Whole rock geochemistry A) Te-Se data and B) Te-Au data, for the Cononish deposit, Scotland, compared with other gold deposits in orogenic belts (circles), bulk continental crust and mantle, and local Dalradian metasediment host-rocks. Where specified, intrusion-related orogenic gold deposits are plotted separately with square symbols, although appear to follow the same trends. Some notable deposits are specifically named. Cononish and Dalradian metasediment data were analysed by OMAC for Scotgold using fire assay-AA for Au and four acid digest and ICP-OES/AES/MS procedures for Te and Se (Hill, 2014). Most other data are from the OSNACA dataset (Brauhart et al., 2017), except: Kirkland Lake, Larder Lake-Cadillac data (Ispolatov et al., 2008); Muruntau (Koneev et al., 2005); Mt Charlotte (Mueller, 2015); continental crust (Wedepohl, 1995; Rudnick and Gao, 2014); mantle (Palme and O'Neil, 2014).

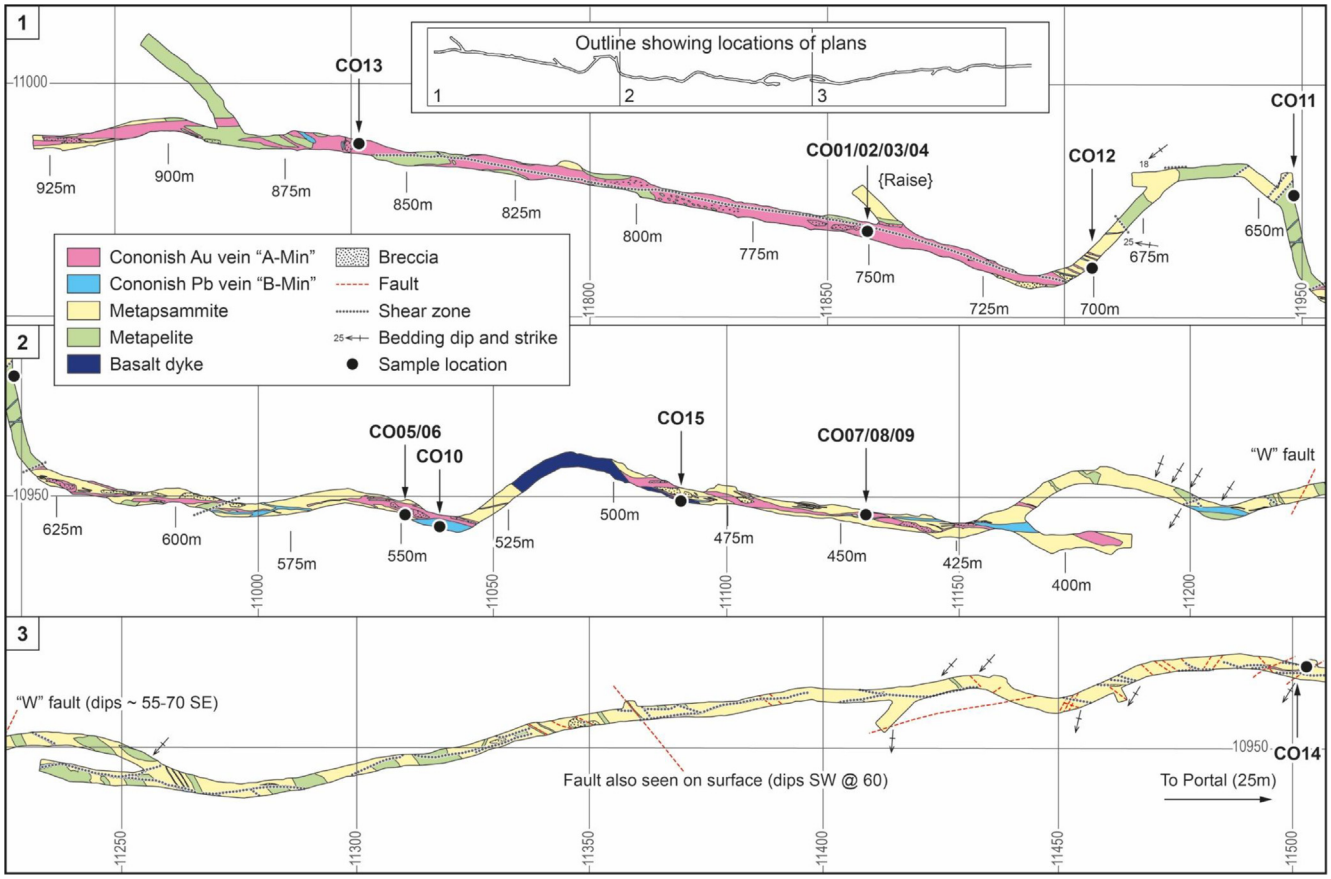

Fig. 2. Simplified mine plan of the 400 mL adit level adapted from plans held by Scotgold Plc, showing the two veins mapped within the deposit and locations of samples taken in this study.

4. Results

4.1. Vein stages

The Cononish Au-Ag vein is predominantly formed from massive milky white quartz, with minor pyrite, chalcopyrite, and galena. Through examining crosscutting relationships, textures and mineral associations (Fig. 3), a detailed paragenesis has been determined (Spence-Jones, 2013) (Fig. 4):

4.1.1. Stage 1 – Early quartz veining

The majority (up to an estimated 70–80% by volume) of the multigenerational vein is an early quartz-cemented breccia and is classified as Stage 1. This comprises a milky white quartz-dominated matrix-supported breccia (Fig. 3A). The clasts (up to ~80 cm) are composed of silicified host rocks that are significantly rotated in relation to the orientation of fabrics in the host lithologies. The milky quartz is formed of coarse 1–2 cm crystals cut by a multitude of fine 50–1000 μm stringer veins observed in thin section due to their fluid inclusion trails. These veins are in optical continuity with the enclosing crystals. In the adit this breccia is most highly developed in the footwall of the Eas Anie fault.

4.1.2. Stage 2 – Early Au-Ag mineralisation

Coarse, up to 2 cm, euhedral cubic pyrite crystals occur within the early quartz veins in sulfide-rich pods that range in size from 1 cm to up to 30 cm. These pods are hosted within the quartz vein and also form 1 to 10 cm halos around altered clasts. This early euhedral pyrite is interpreted to have formed later than the Stage 1 quartz veinlets since the pyrite has not been crosscut by any of the quartz veinlets nor does it contain any quartz inclusions.

The coarse pyrite crystals host the earliest Au-Ag (± Cu, Pb) mineralisation within fractures and as trails of inclusions. The fractures contain the assemblage hessite (Ag_2Te) + Au-Ag alloy + galena ± altaite (PbTe) ± chalcopyrite (Fig. 3D) that is diagnostic of the Au-Ag mineralisation.

4.1.3. Stages 3–4 – Evolution of the Au-Ag mineralisation

The vein material formed during Stages 1 and 2 is cross cut and comminuted by later narrow, 0.5–10 cm-wide veinlets of dark grey recrystallized quartz with sulfide that typically form anastomosing arrays up to half a metre wide and often show shear displacement (Fig. 3A/C). These veins host abundant chalcopyrite and galena with subordinate pyrite, sphalerite, calcite, and minor Au-Ag alloy and hessite (Fig. 3C and E). The sulfides comprise > 50% by volume of stage 3–4 vein mineralogy. Stage 3 and 4 veins have been separated to represent end-members of a continuous trend based on the relative proportions of chalcopyrite and galena, progressing from 90% galena to 90% chalcopyrite (the latter often observed with calcite). The Stage 3 galena-rich veins are inferred to be earlier as they are crosscut by later calcite-chalcopyrite veins. Stage 4 veins may contain acanthite (Ag_2S) instead of hessite. Whether a particular vein in an individual sample is Stage 3 or 4 is often difficult to decide due to variations in mineralogy along the veins. In practice, the distinction is made on the relative proportions of galena and chalcopyrite and the Au-Ag alloy composition.

4.1.4. Stage 5 – Post ore alteration

In one location (Sample CO13, Fig. 2) in the underground workings, referred to as the "666 zone" by miners, earlier stage 1–4 veining is strongly altered to magnetite and hematite, and calcite veining is pervasive. The 666 zone is localised to a narrow area in the roof of the adit

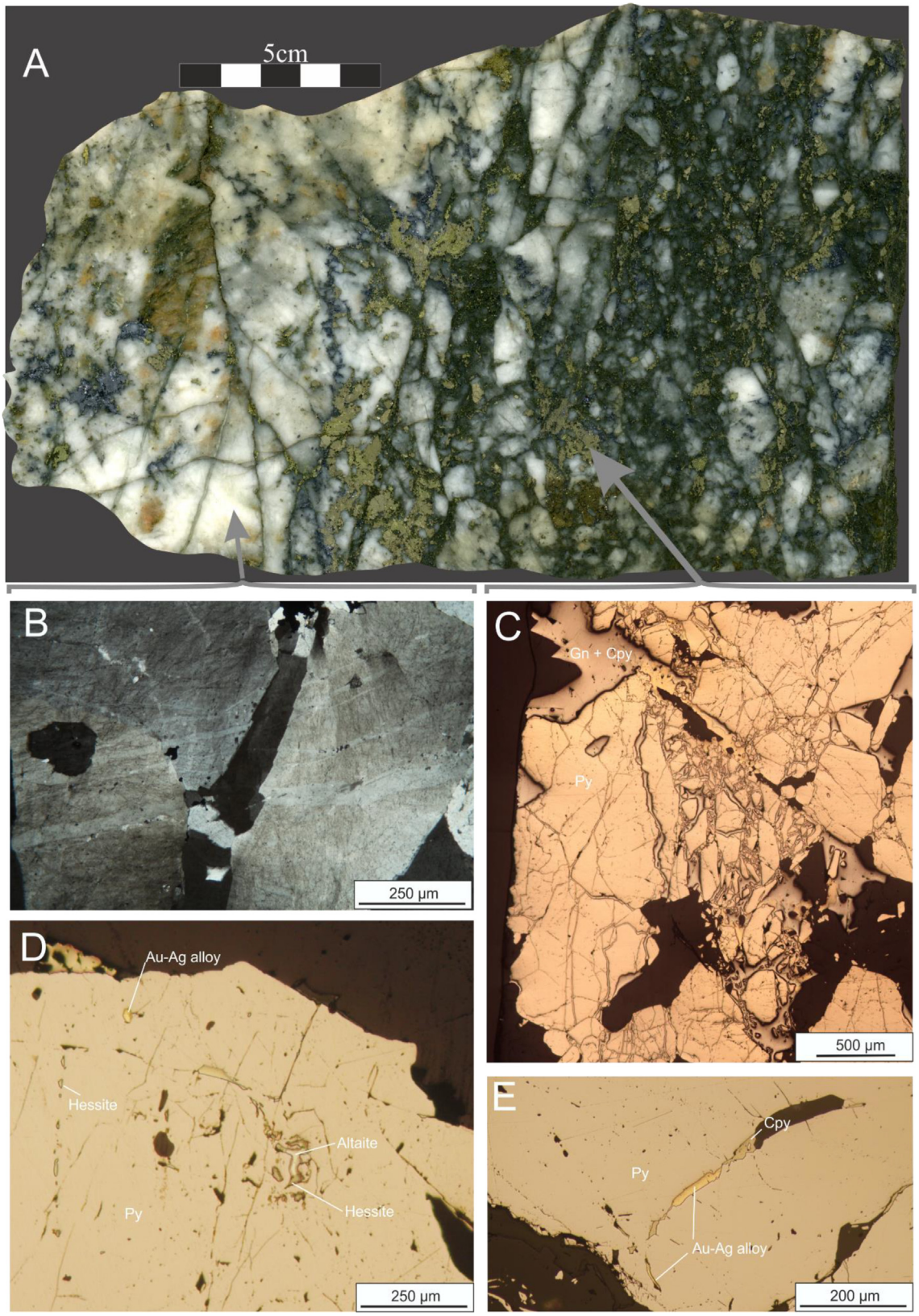

Fig. 3. Textures of the Cononish Vein. A) Polished slab of part of sample CO03 showing the typical ore textures closest to the fault. Stage 1 quartz is brecciated by multiple crosscutting Stage 3/4 veining. The right-hand side of the block is the fracture along the Cononish fault plane. The arrows relate the thin section textures to hand specimen textures. B) Transmitted light XPL image of sample CO03 showing stage 1 coarse vein quartz preserving the early veinlets through inclusion abundance variation between the generations. C) Composite reflected PPL image of sample CO06 showing brittle fracturing and veining of early pyrite (Py) by later Stage 3/4 galena (Gn) and chalcopyrite (Cpy). D) Reflected light PPL image of a coarse pyrite (Py) illustrating the inclusions trail textures typical of Stage 2, sample CO02. E) Reflected PPL image of a coarse pyrite (Py) fractured and veined by Stage 3/4 chalcopyrite (Cpy) showing strong association with coarse Au-Ag alloy, sample CO06.

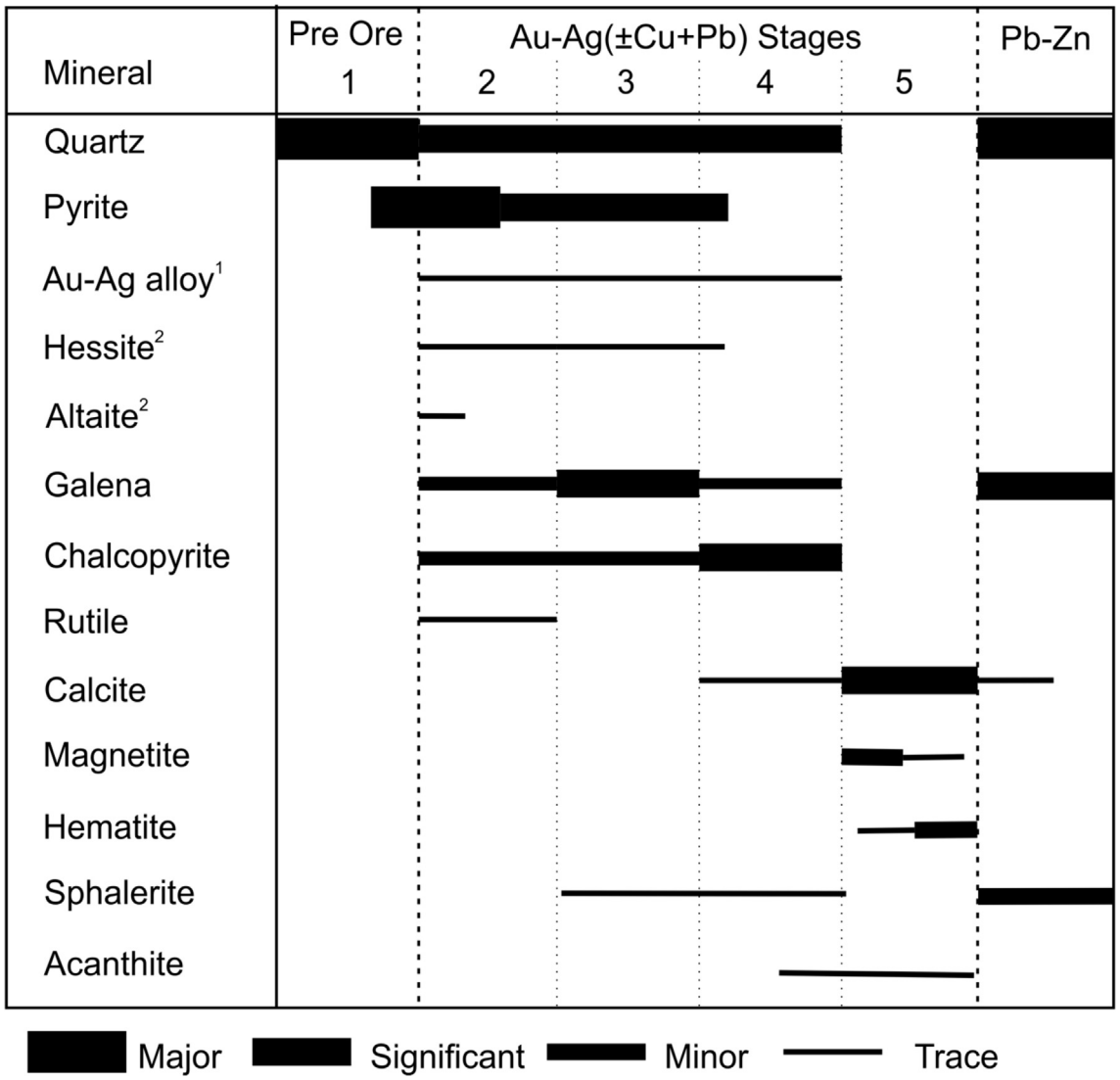

Fig. 4. Paragenesis for the Cononish Au-Ag (± Cu, Pb) vein and later cross-cutting Pb-Zn vein. Estimated relative mineral proportions are shown by width of the bar. [1]Au content of the alloy is observed to decrease over time. [2]Abundance of tellurides decreases from stage 2 with very few tellurides observed in stage 3 mineralisation.

and appears unrelated related to the stage 1–4 mineralising event but rather is a post-ore alteration. The relationship of Stage 5 to the late stage 6 veining is not known and the earlier placement in the paragenesis is based on the lack of vuggy textures and greater textural and mineralogical similarity to stages 1–4 than the brittle late stage 6 veining.

4.1.5. Stage 6 – Pb-Zn Vein

The late Pb-Zn veining clearly crosscuts stages 1–4, often at a different orientation, and comprises predominantly sugary fragmented vuggy quartz with abundant coarse euhedral galena and yellow sphalerite. No Au-Ag alloy occurs in Stage 6 and it is not discussed further.

4.2. Au-Ag alloy composition and association

The gold and silver concentrations in 215 individual Au-Ag alloy grains in polished thin section were measured by SEM-EDX (Spence-Jones, 2013; Full dataset in Supplementary Data). Grain major axis ranges from 1 to 400 μm, but most grains are small with a median of 15 μm. The median aspect ratio is 2. Some grains are highly elongated along fractures (up to 400 × 5 μm), but the few grains with the largest area (20000–50000 μm^2) are fairly equant with aspect ratio of 2–5. The composition of the gold ranges from ~10% to ~90 wt% Ag, i.e. from gold to silver rich, through what was formerly termed electrum (Fig. 5). There is no evidence for variations in composition within individual grains that are greater than analytical uncertainty. However, in general the more silver-rich grains tend to be smaller, with median major axis length of 10 μm for grains with > 60 wt% Ag, compared to 20 μm for grains with < 60 wt% Ag.

The broad range in grain composition is in contrast to many hydrothermal gold deposits which, with the exception of epithermal deposits, show much narrower compositional ranges, e.g. Au-Ag alloy ranging between 75 and 90% Au, or 60–90% Au from placer deposits (Chapman and Mortensen, 2016; Chapman et al., 2010; Morrison et al., 1991). Narrower ranges in composition (10–20% variation) occur within individual samples (Fig. 5), indicating that the Au-Ag alloy formed under similar conditions within a thin section sized sample of the vein. This is consistent with the textural observations that later stages of mineralisation have overprinted the earlier stages, unless minerals were shielded from the late fluid as inclusions within early minerals.

Whilst is not possible to unequivocally allocate every Au-Ag alloy grain to a mineralisation stage it is possible to define its association with other minerals that link it to the stages in the paragenesis (Fig. 6). There is a distinct association of the Au-rich alloy (gold) grains with hessite, whereas

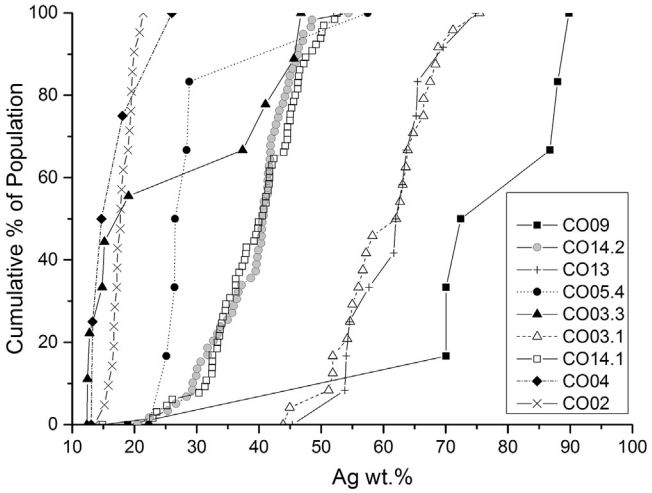

Fig. 5. Cumulative plot of the Ag wt% proportion of Au-Ag alloy grains measured in this study (n = 215) shown as populations of grains within an individual thin section. Each sample recorded a distinct and variable distribution of grain compositions dependent on the stages of the paragenetic sequence sampled. A limited number of the thin sections, such as CO03.3, CO04 and CO09, show a bimodal distribution of Au-Ag alloy composition that can be correlated with the observation that they contained two or more distinct gold bearing stages of the paragenesis.

Ag-rich alloy (silver) is strongly associated with chalcopyrite. Galena is associated with the whole range of Au-Ag alloy compositions.

4.3. Sulfur isotope data

Results of 16 pyrite S-isotope analyses are given in Table 1 and plotted along with the combined published S-isotope dataset for Connish in Fig. 7A. These show a range of $\delta^{34}S$ values from −2 to +11.4‰. Samples for this study were taken from coarse pyrite crystals that are temporally constrained in the paragenetic sequence described above (Fig. 8). This reveals a trend of increasing $\delta^{34}S$ through the paragenetic sequence (Fig. 7B). Two samples that could relate to either Stage 3 or 4, as they show mineralogical and textural features of both stages, were plotted as Stage 3.5. The sample from Hill et al. (2013) with a $\delta^{34}S$ of −2‰, which was not paragenetically constrained in this study, is assumed to belong to Stage 2, and gives a lower value for this stage. If it included in the statistics, mean and standard deviation for Stage 2 would be +0.7 ± 1.8‰. To avoid bias in the results, the position of the samples in the paragenesis was determined during sampling before analysis was undertaken.

5. Discussion

5.1. Evolution of Au-Ag alloy composition

In a hydrothermal system Au-Ag alloy compositions are controlled through the ratio of chemical activities aAg/aAu (Gammons and Williams-Jones, 1995). Where an additional Ag phase such as Ag_2S or Ag_2Te is saturated then the activity of Ag will be buffered by these

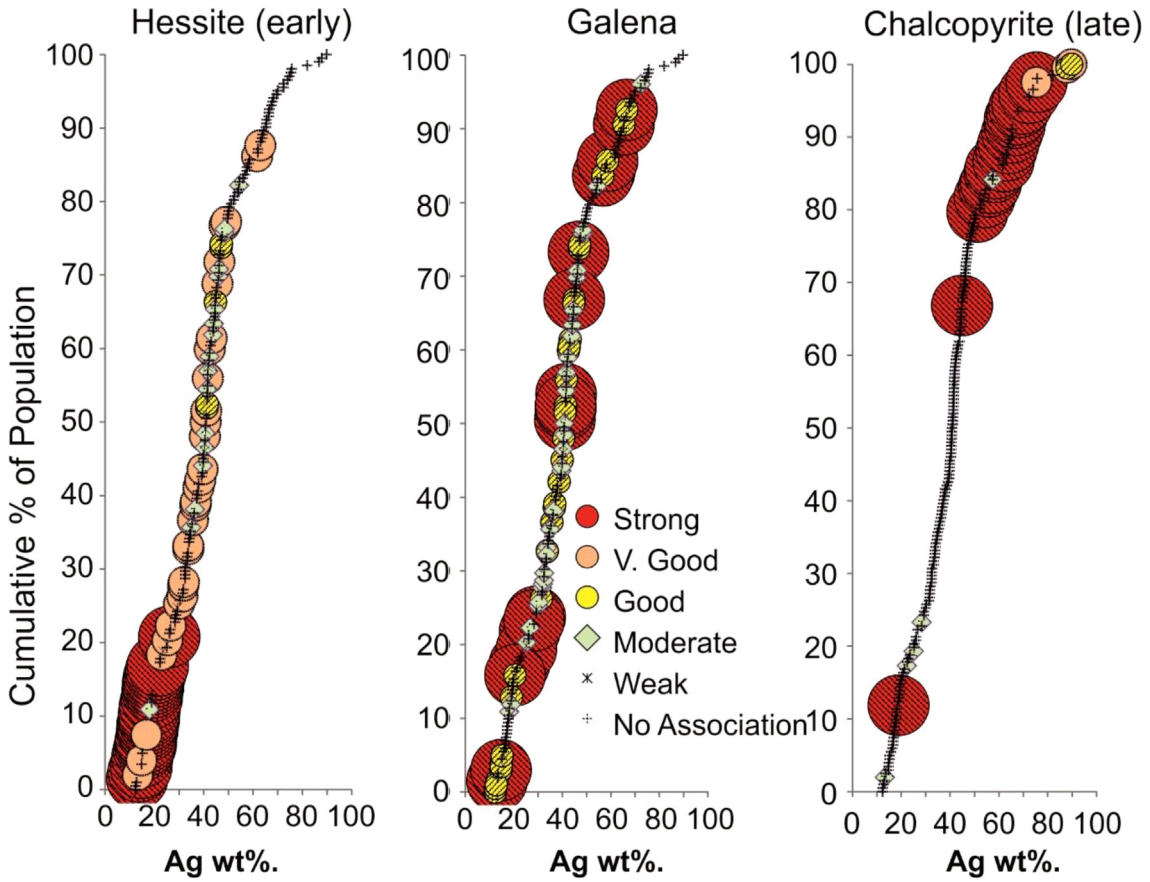

Fig. 6. Cumulative plot of the composition of all Au-Ag alloy grains with observed mineral associations for hessite, chalcopyrite and galena. The symbol indicates the qualitative strength of the association: Strong association indicates the phases are clearly related, for example intergrown mineral textures. Moderate association indicates minerals that are observed together in a fracture or a veinlet. Weak association represents a tenuous link, such as Au-Ag alloy occurring in veins sets that contain the associated mineral distally. No association indicates the minerals were not observed with Au-Ag alloy in a vein.

Table 1
Paragenetically-constrained pyrite sulfur isotope data at Cononish deposit.

Sample	Description	$\delta^{34}S$ (‰)	Stage sampled
CO02a	Stage 2 coarse pyrite in white massive stage 1 quartz vein.	1.3	2
CO02b	Stage 2 coarse pyrite in white massive stage 1 quartz vein.	1.7	2
CO02*	Stage 2 coarse pyrite in white massive stage 1 quartz vein.	1.8	2
	Mean and standard deviation	1.6±0.3	
CO14a*	Sheared stage 3 vein with pyrite, minor Gal > Cpy present.	4.7	3
CO05.2c	Coarse pyrite crosscutting stage 1 and 2, Gal > Cpy.	6.6	3
CO05.2a	Coarse pyrite crosscutting stage 1 and 2, Gal > Cpy.	6.7	3
CO05.2b	Coarse pyrite crosscutting stage 1 and 2, Gal > Cpy.	6.7	3
CO14b*	Stage 3 vein with pyrite crosscutting stage 1 and 2, minor Gal > Cpy.	7.2	3
CO06c	Pyrite veinlet in sulfide rich quartz crosscutting stage 1 and 2.	8.5	3
	Mean and standard deviation	6.7±1.2	
CO06a	Coarse pyrite in stage 3/4 vein (Gal ≈ Cpy).	8.2	3/4
CO06b	Coarse pyrite in stage 3/4 vein (Gal ≈ Cpy).	8.3	3/4
	Mean and standard deviation	8.3±0.1	
CO05.1	Coarse pyrite in veinlet hosting Cpy > Gal.	8.3	4
CO05*	Coarse pyrite from narrow sulfide rich shear hosting Cpy > Gal.	8.9	4
CO03c*	Pyritic veinlet hosting abundant Cpy > Gal.	11.0	4
CO03a	Pyrite veinlet hosting abundant Cpy > Gal.	11.2	4
CO03b	Pyrite veinlet hosting abundant Cpy > Gal.	11.4	4
	Mean and standard deviation	10.2±1.4	

* Data previously reported in Hill et al. (2013) assigned to the revised paragenesis here.

phases (Gammons and Williams-Jones, 1995). Whilst galena can accommodate some Ag it does so through coupled substitution with Sb or Bi (e.g. Renock and Becker, 2011) and as these elements are low in Cononish ores, ~1 ppm and < 30 ppm respectively, Ag content in galena is expected to be minor and not an important buffering phase for Ag. This is supported by preliminary LA-ICP-MS data which suggest galena Ag content is ~100 ppm. So, in the case of coexistence of Au-Ag alloy with hessite, as at Cononish, the Au-Ag alloy Ag-content is controlled through the reaction (Gammons and Williams-Jones, 1995):

$$Ag_{alloy} + \frac{1}{4}Te_{2(g)} = \frac{1}{2}Ag_2Te_{(s)} \quad (1)$$

And

$$aAg_{alloy} = K_{eq1}^{-1} \cdot a_{Te_2}^{-0.25} \quad (2)$$

(where K is the equilibrium constant of the reaction in Eq. (1).)

Thus, the composition of Au-Ag alloy in equilibrium with an Ag_2Te saturated fluid will be dependent on the activity of Te_2 in the system. If $aTe_{2(g)}$ is high then large proportions of hessite will precipitate removing Ag available to the Au-Ag alloy and keeping aAg low. This will produce Au-rich Au-Ag alloy as the buffered ratio of aAg/aAu will be high. At Cononish in Stage 2, hessite is abundant along with Au-rich alloy; 90–75% Au (Fig. 6). In Stages 3 and 4, the abundance of hessite decreases, and is absent in late Stage 4 mineralisation, and here associated Au-Ag alloy grains have higher silver contents; 10–75% Au (Fig. 6). In late Stage 4 veinlets, acanthite occurs instead of hessite. It is interpreted that high aTe_2 in the early fluid controlled the composition of the Au-Ag alloy and a progressive decrease in aTe_2 over time led to the deposition of progressively more Ag-rich alloy until aTe_2 decreased sufficiently in late Stage 4 that acanthite was deposited. The decrease in galena abundance from Stage 3–4 would also act to increase Ag content in the Au-Ag alloy, but since the Ag content of galena is low, this effect was negligible.

The relationship between alloy composition and Te fugacity has been quantified as a function of temperature by Afifi et al. (1988), who show that fugacity of Te in a system is related to the mole fraction of Ag (X_{Ag}) in the alloy by:

$$\log f_{Te_2} = \left[\frac{1}{4.576T}\right] \cdot [\Delta G_T^o(Ag_2Te) - 18.302.\ T.\ Log\ X_{Ag} + 4(1-X_{Ag})^2 \cdot (5650 - 1600(1-X_{Ag}) - 1.375T)] \quad (3)$$

assuming unit activity of Ag_2Te in hessite and ideal mixing of Au and Ag in the alloy.

This shows that to reduce Te activity with time *via* temperature change, a temperature *rise* would have been required which would seem unlikely given the limited range of fluid inclusion temperatures of 290–340 °C (Curtis et al., 1993). Therefore, our data more likely indicate a change in fluid source.

5.2. Sulfur sources

The evolution in $\delta^{34}S_{pyrite}$ from early pyrite with $\delta^{34}S$ of −2 to 2‰ towards a late stage pyrite with values up to +11.4‰ represents a significant, and statistically robust, shift in the sulfur isotope composition of the fluid, which is interpreted as a change of the sulfur source. Hill et al. (2013) examined the $\delta^{34}S$ of the local stratigraphy and discussed potential sulfur sources for the Au-Ag mineralisation at Cononish. They demonstrated that it is possible to produce the full range of S-isotope values at Cononish, either by mixing of sulfur from different units in the local stratigraphy, or by mixing of magmatic sulfur with metasedimentary derived sulfur with $\delta^{34}S \geq +12$‰ from the Ben Eagach Schist SEDEX-bearing stratigraphic units. Hill et al. (2013) advocated the latter scenario, given the timing of the mineralisation. The age of the Cononish Au-bearing veins of ~407 Ma (Rice et al., 2012) is

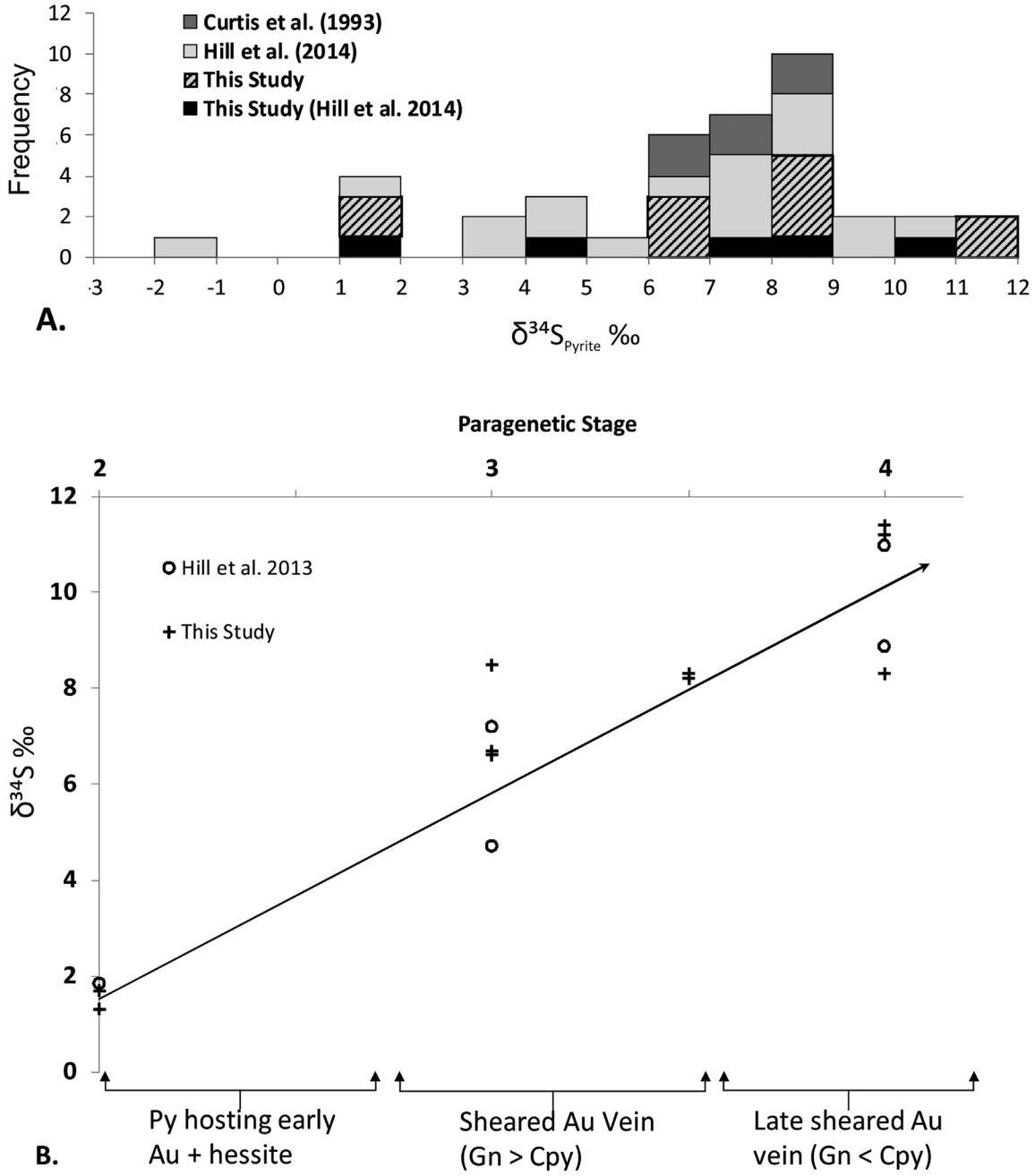

Fig. 7. A. Histogram of compiled pyrite $\delta^{34}S$ for the Cononish deposit. B. Pyrite $\delta^{34}S$ vs. paragenetic stage.

identical, within error, to the Inner Starav Granite U-Pb zircon dated at 407 ± 2 Ma (Appleby, 2007) and 408 ± 0.5 Ma (Neilson et al., 2009), the youngest portion of the Etive Pluton Complex situated 15 km to the NW across the Ericht-Laidon Fault. In addition, the $\delta^{34}S$ of the early pyrite at Cononish is almost identical to that of sulfides from the Etive granite which average +2.1‰ (Lowry et al., 2005), and to the Sron Garbh appinite-diorite body (+1.0 to +4.8‰) that lies ~5 km to the northeast (Graham et al., 2017). Curtis et al. (1993) suggested magmatic fluid input on the basis of fluid oxygen and hydrogen isotope ratios derived from measurements on quartz. Furthermore, the mineralisation formed > 60 Ma later than peak metamorphism at ~470 Ma (Stephenson et al., 2013), so it is difficult to argue that it formed from regional metamorphic fluids, even acknowledging a "deeper-later" model for metamorphic fluid release which, at most, delays fluid release from depth by 50 Ma (Stüwe, 1998).

The paragenetically constrained pyrite $\delta^{34}S$ data extend the mixing scenario proposed by Hill et al. (2013), now showing that the range of data can be interpreted as early magmatic sulfur progressively mixing over time with metasedimentary sulfur. The latter could be explained by metasedimentary sulfur being released by contact metamorphism and/or greater degrees of fluid-rock interaction during the evolution of the system. The source of the metasedimentary sulfide in this model must be the Easdale Subgroup; specifically, the highest $\delta^{34}S$ values reached can only be explained by sulfur being sourced from Ben Eagach Schist SEDEX sulphides which range up to +28‰, average +20‰ (Moles et al., 2014). The Easdale Subgroup is stratigraphically above the host rocks of the Cononish deposit, however it is inferred to underlie the deposit on the opposing limb of the Beinn Chuirn Anticline (Hill et al., 2013). To produce the same trend of increasing $\delta^{34}S$ values over time from a purely metasedimentary-sourced hydrothermal system, without magmatic fluid involvement, would require sourcing of fluids from different (yet possibly adjacent) metasedimentary reservoirs

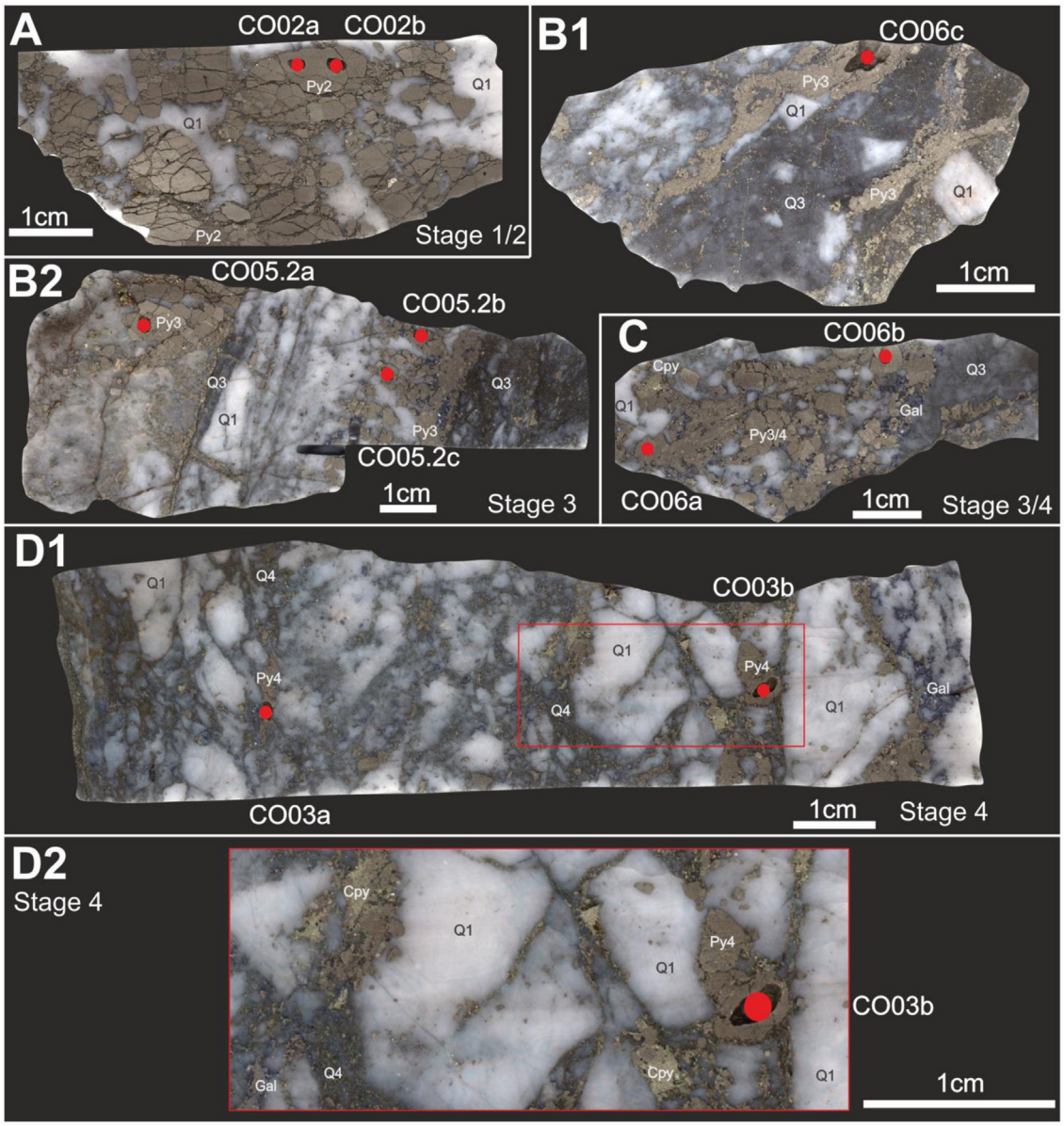

Fig. 8. Scans of polished slabs showing the location of drilled sulfur isotope samples (red circles) and the interpreted stage of the pyrite sampled. A) Early Stage 1 milky quartz with coarse pyrite of stage 2. B1) Stage 3 pyritic veinlets with trace galena and chalcopyrite on the margins of a dark pyritic quartz vein brecciating stage 1 quartz. B2) Coarse pyrite crosscutting the margin of a dark pyritic quartz vein crosscutting massive stage 1 quartz. C) Coarse Stage 3/4 pyrite crosscutting stage 1 quartz with approximately equal proportions of coarse galena and chalcopyrite. D1) Multiple coarse Stage 4 pyrite (with coarse chalcopyrite and minor galena) and pyritic quartz veins cross cutting/brecciating Stage 1 quartz. D2 shows an enlarged proportion (red box in D1) showing the coeval intergrowths of pyrite and chalcopyrite.

within the Easdale Subgroup that range from −15 to +28‰ (Hill et al., 2013). Furthermore, it would necessitate changing sulfur sources or fluid pathways through the metasedimentary sequence during deposit formation with later fluid somehow becoming isolated from the initial sulfur source. Whilst not impossible, we argue that this option seems rather more contrived given the timing of the mineralisation.

5.3. Implications for the tellurium source

The decrease in tellurium activity coupled with an increase in $\delta^{34}S$ through the formation of the Au-Ag vein suggest a low $\delta^{34}S$ (averaging +1.6‰, but possibly as low as −2‰), Te + Au + Ag enriched initial ore fluid evolved towards a high $\delta^{34}S$ (≥11‰), low Te, Pb + Cu-bearing fluid. The low $\delta^{34}S$ source is interpreted here as a magmatic pulse of fluid, as advocated by Hill et al. (2013) and Curtis et al. (1993), and this implies that the Te is also most likely of magmatic origin. The strong similarity of the Se-Te-Au ratios at Cononish with the Kirkland Lake deposits is notable (Fig. 1). Interestingly, in contrast to the more typical "orogenic" Larder Lake-Cadillac mineralisation, Ispolatov et al. (2008) propose that the distinct metal signature at Kirkland Lake relates to a deep magmatic (alkalic) fluid source.

The earliest Au-Ag-Te mineralisation is hypothesised to represent the introduction of significant volumes of magmatic fluid into brittle structures. It is suggested that this magmatic fluid ascended rapidly out of chemical equilibrium with the Dalradian metamorphic pile through brittle fractures from a blind intrusive crystallising at depth (as suggested by a gravity low that extends beneath the area from the Etive pluton complex; Hill et al., 2013). The evolution away from the strongly Te saturated initial fluid and increase in $\delta^{34}S$ is interpreted as a waning of magmatic fluid input and regaining of geochemical equilibrium with

the Dalradian metasediments by the fluids ascending within the fault.

The alternative explanation of the tellurium-$\delta^{34}S$ evolution with time is that both early and late fluids were sourced from the Dalradian metasedimentary pile, but that different parts of the stratigraphy released fluids at different times. Associations of gold and tellurium are well known in some orogenic gold districts (e.g. Ashanti; Bowell et al., 1990) where there is little evidence of a magmatic fluid input, so in these cases Te may be sourced from metasedimentary or metaigneous units (or simply strongly concentrated on precipitation by specific physicochemical gradients in these systems). Parnell et al. (2017) demonstrate that carbonaceous shales from the Easdale Subgroup contain early diagenetic pyrite enriched in both Au and Te, and could represent a viable source-rock for the mineralisation. However, if the early low-$\delta^{34}S$, high Te + Au fluid at Cononish was sourced from the Dalradian metasediments then, on the basis of its sulfur isotope signature, it would need to come from other Formations in the Easdale Subgroup such as the Ben Lawers Schist, or a restricted subset of the diagenetic sulfides of the Ben Eagach schist (Hill et al., 2013) – units very close to those supplying the late high-$\delta^{34}S$ signature. This would require a highly specific contact-metamorphically sourced scenario to enable the origin and evolution of these fluids from adjacent units.

6. Conclusions

The Cononish Au-Ag deposit formed as the result of an early fluid pulse from a low-$\delta^{34}S$ (~1‰), high Te + Au + Ag source that evolved towards a high-$\delta^{34}S$ (≥11‰), low Te, Pb + Cu bearing fluid with time. The low $\delta^{34}S$ source is interpreted here as a magmatic pulse of fluid and the evolution away from the strongly Te-saturated initial fluid is interpreted as a waning of magmatic fluid input and regaining of geochemical equilibrium with the Dalradian metasediments. Whilst not all examples of high Te-enrichment in orogenic gold deposits can be attributed to a magmatic fluid input, in *some* orogenic Au deposits it would seem that high Te *is* a signature of magmatic fluid input. The identification of specific pluses of Te enrichment during formation is an additional tool towards discrimination of a subclass of orogenic gold deposits that have formed through distal or otherwise cryptic magmatic processes.

Acknowledgements

NH was funded by the Natural Environment Research Council (NERC) Open CASE studentship NE/H017755/1 with Scotgold Resources Ltd. Scotgold are acknowledged for financial and logistical field support and access to company information. S-isotope analyses were carried out at SUERC under NERC Isotope Facilities grant IP–1317–0512. AJB is funded by NERC support of the Isotope Community Support Facility. GRTJ is supported by NERC Minerals Security of Supply (SoS) grant NE/M010848/1 Tellurium and Selenium Cycling and Supply (TeaSe). We thank Manuel Keith for carrying out some preliminary LA-ICP analyses on galena and are grateful to an anonymous reviewer and Clive Rice for their perceptive comments which helped us improve the manuscript.

Appendix A. Supplementary data

Supplementary data associated with this article can be found, in the online version, at https://doi.org/10.1016/j.oregeorev.2018.05.014.

References

Afifi, A.M., Kelly, W.C., Essene, E.J., 1988. Phase relations among tellurides, sulfides, and oxides; I, thermochemical data and calculated equilibria. Econ. Geol. 83, 377–394.
Appleby, K.S., 2007. The Origin and Evolution of granites: an in Situ study of Zircons from Scottish Caledonian Intrusions. Unpublished PhD thesis. University of Edinburgh.
Bowell, R.J., Foster, R.P., Stanley, C.J., 1990. Telluride mineralization at Ashanti gold mine. Ghana: Min. Mag. 54, 617–627.
Brauhart, C.W., Grunsky, E.C., Hagemann, S.G., 2017. Magmato-hydrothermal space: a new metric for geochemical analysis of metallic ore deposits. Ore Geol. Rev. 86, 867–895.
Burrows, D.R., Spooner, E.T.C., 1989. Relationships between Archean gold quartz vein-shear zone mineralization and igneous intrusions in the Val d'Or and Timmins areas, Abitibi subprovince Canada. Econ. Geol. Monogr. 6, 424–444.
Chapman, R.J., Mortensen, J.K., 2016. Characterization of gold mineralization in the northern Cariboo Gold District, British Columbia, Canada, through integration of compositional studies of lode and detrital gold with historical placer production: A template for evaluation of orogenic gold. Econ. Geol. 111, 1321–1345.
Chapman, R.J., Mortensen, J.K., Crawford, E.C., Lebarge, W., 2010. Microchemical studies of placer and lode gold in the Klondike district, Yukon, Canada: 1. Evidence for a small, gold-rich, orogenic hydrothermal system in the Bonanza and Eldorado Creek area. Econ. Geol. 105, 1369–1392.
Craw, D., Chamberlain, C.P., 1996. Meteoric incursion and oxygen fronts in the Dalradian metamorphic belt, southwest Scotland: a new hypothesis for regional gold mobility. Miner. Depos. 31, 365–373.
Curtis, S.F., Pattrick, R.A.D., Jenkin, G.R.T., Fallick, A.E., Boyce, A.J., Treagus, J.E., 1993. Fluid inclusion and stable isotope study of fault-related mineralization in Tyndrum area, Scotland. Trans Inst. Min. Metall. Sec. B Appl. Earth Sci. 102, B39–B47.
Earls, G., Patterson, R.T.G., Clifford, J.A., Meldrum, A.H., 1992. The geology of the cononish gold silver deposit, Grampian Highlands of Scotland. In: Bowden, A.A. (Ed.), The Irish Minerals Industry 1980–1990. Irish Association for Econ Geol, pp. 89–103.
Gammons, C.H., Williams-Jones, A.E., 1995. Hydrothermal geochemistry of electrum – thermodynamic constraints. Econ. Geol. 90, 420–432.
Goldfarb, R.J., Groves, D.I., 2015. Orogenic gold: Common or evolving fluid and metal sources through time. Lithos 233, 2–26.
Goldfarb, R.J., Snee, L.W., Pickthorn, W.J., 1993. Orogenesis, high-T thermal events, and gold vein formation within metamorphic rocks of the Alaskan cordillera. Min Mag. 57, 375–394.
Goldfarb, R.J., Hart, C., Miller, M., Miller, L., Farmer, G.L., Groves, D.I., 2000. The Tintina Gold Belt – A global perspective. In: Tucker, T.L., Smith, M.T. (Eds.), The Tintina gold belt – Concepts, exploration, and discoveries. British Columbia and Yukon Chamber of Mines Spec, pp. 5–34.
Goldfarb, R.J., Baker, T., Dubé, B., Groves, D.I., Hart, C.J.R., Gosselin, P., 2005. Distribution, character, and genesis of gold deposits in metamorphic terranes. Econ. Geol. 100th Anniv. 407–450.
Goldfarb, R.J., Berger, B.R., George, M., Seal, R.II, 2016, Tellurium, Chapter R of Schulz, K.J., Bradley, D.C., DeYoung, J.H.Jr., Seal, R.R.II, eds, Critical Mineral Resources of the United States, Economic and Environmental Geology and Prospects for Future Supply: U.S. Geological Survey Professional Paper 1802, 27 p.
Graham, S.D., Holwell, D.A., McDonald, I., Jenkin, G.R.T., Hill, N.J., Boyce, A.J., Smith, J., Sangster, C., 2017. Magmatic Cu-Ni-PGE-Au sulfide mineralisation in alkaline igneous systems: An example from the Sron Garbh intrusion, Tyndrum. Scotland. Ore Geol. Rev. 80, 961–984. http://dx.doi.org/10.1016/j.oregeorev.2016.08.031.
Groves, D.I., Goldfarb, R.J., Gebre-Mariam, M., Hagemann, S.G., Robert, F., 1998. Orogenic gold deposits: a proposed classification in the context of their crustal distribution and relationship to other gold deposit types. Ore Geol. Rev. 13 (1998), 7–27.
Groves, D.I., Goldfarb, R.J., Robert, F., Hart, C.J., 2003. Gold deposits in metamorphic belts: overview of current understanding, outstanding problems, future research, and exploration significance. Econ. Geol. 98, 1–29.
Hammond, N.Q., Robb, L.J., Foya, S., Ishiyama, D., 2011. Mineralogical, fluid inclusion and stable isotope characteristics of Birimian orogenic gold mineralization at the Morila Mine, Mali, West Africa. Ore Geol. Rev. 39, 218–229.
Hart, C., Goldfarb, R., 2005, Distinguishing intrusion-related from orogenic gold systems: New Zealand Minerals Conference Proceedings, 2005, 125–133.
Hill, N.J., 2014. Development of a genetic model for targeting gold mineralisation in the Dalradian Supergroup, Scotland. PhD thesis. University of Leicester.
Hill, N.J., Jenkin, G.R.T., Boyce, A.J., Sangster, C.J.S., Catterall, D.J., Holwell, D.A., Naden, J., Rice, C.M., 2013. How the Neoproterozoic S-isotope record illuminates the genesis of vein gold systems: an example from the Dalradian Supergroup in Scotland. In: Jenkin, G.R.T., Lusty, P.A.J., McDonald, I., Smith, M.P., Boyce, A.J., Wilkinson, J.J. (Eds.), Ore Deposits in an Evolving Earth. Geol. Soc. London, Spec. Pub., pp. 213–247.
Ispolatov, V., Lafrance, B., Dubé, B., Creaser, R., Hamilton, M., 2008. Geologic and structural setting of gold mineralisation in the Kirkland Lake-Larder Lake gold belt, Ontario. Econ. Geol. 103, 1309–1340.
Kerrich, R., 1989. Archean gold – Relation to granulite formation or felsic intrusions. Geology 17, 1011–1015.
Kerrich, R., Wyman, D., 1990. Geodynamic setting of mesothermal gold deposits – an association with accretionary tectonic regimes. Geology 18, 882–885.
Koneev, R., Ignatikov, E., Turesebekov, A., Aripov, U., Khalmatov, R., Kodirov, O., Usmanov, M., 2005. Gold ore deposits of Uzbekistan: geochemistry and nanomineralogy of tellurium and selenium. Geochem. Mineral. Petrol. 43, 102–107.
Large, R.R., Danyushevsky, L., Hollit, C., Maslennikov, V., Meffre, S., Gilbert, S., Bull, S., Scott, R., Emsbo, P., Thomas, H., et al., 2009. Gold and trace element zonation in pyrite using a laser imaging technique: implications for the timing of gold in orogenic and Carlin-style sediment-hosted deposits. Econ. Geol. 104, 635–668.
Lowry, D., Boyce, A. J., Fallick, A. E., Stephens, W. E., and Grassineau, N. V., 2005, Terrane and basement discrimination in northern Britain using sulphur isotopes and mineralogy of ore deposits, in McDonald, I., Boyce, A. J., Butler, I. B., Herrington, R. J., and Polya, D. A., eds., Mineral deposits and Earth evolution, Geological Society Special Publication: 248., 133–151.
McFarlane, C.M., Mavrogenes, C.M., Lentz, D., King, K., Holcombe, R., 2011. Geology and

Intrusion-related affinity of the Morila Gold Mine, southeast Mali. Econ. Geol. 106, 727–750.
Moles, N.R., Boyce, A.J., Fallick, A.E., 2014. Abundant sulfate in the Neoproterozoic ocean: implications of constant $\delta^{34}S$ of barite in the Aberfeldy SEDEX deposits, Scottish Dalradian. Special Publications In: Jenkin, G.R.T., Lusty, P.A.J., McDonald, I., Smith, M.P., Boyce, A.J., Wilkinson, J.J. (Eds.), Ore Deposits in an Evolving Earth. Geological Society of London, pp. 189–212. http://dx.doi.org/10.1144/SP393.7.
Morrison, G.W., Rose, W.J., Jaireth, S., 1991. Geological and geochemical controls on the silver content (fineness) of gold in gold-silver deposits. Ore Geol. Rev. 6, 333–364.
Neilson, J.C., Kokelaar, B.P., Crowley, Q.G., 2009. Timing, relations and cause of plutonic and volcanic activity of the Siluro-Devonian post-collision magmatic episode in the Grampian terrane. Scotland. J. Geol. Soc. 166, 545–561.
Mueller, A.G., 2015. Structure, alteration and geochemistry of the Charlotte quartz vein stockwork, Mt Charlotte gold mine, Kalgoorlie, Australia: time constraints, down-plunge zonation, and fluid source. Miner. Deposita 50, 221–244.
Palme, H., O'Neil, H.St.C, 2014. Cosmochemical estimates of mantle composition, 2nd edition. Elsevier, pp. 1–39 Chapter 1 in Treatise on Geochemistry.
Parnell, J., Perez, M., Armstrong, J., Bullock, L., Feldmann, J., 2017. A black shale protolith for gold-tellurium mineralisation in the Dalradian Supergroup (Neoproterozoic) of Britain and Ireland. Appl. Earth Sci. (Trans. Inst. Min. Metal. B) 126, 161–175. http://dx.doi.org/10.1080/03717453.2017.1404682.
Pattrick, R.A.D., Boyce, A., MacIntyre, R.M., 1988. Gold-silver vein mineralization at Tyndrum, Scotland. Mineral. Petrol. 38, 61–76.
Pettke, T., Diamond, L.W., Villa, I.M., 1999. Mesothermal gold veins and metamorphic devolatilization in the northwestern Alps: the temporal link. Geology 27, 641–644.
Phillips, G.N., Powell, R., 2010. Formation of gold deposits: a metamorphic devolatilization model. J. Metam. Geol. 28, 689–718.
Pitcairn, I.K., Teagle, D.A.H., Craw, D., Olivo, G.R., Kerrich, R., Brewer, T.S., 2006. Sources of metals and fluids in orogenic gold deposits: insights from the otago and alpine schists, New Zealand. Econ. Geol. 101, 1525–1546.
Pitcairn, I.K., Craw, D., Teagle, D.A.H., 2014. The gold conveyor belt: Large-scale gold mobility in an active orogen. Ore Geol. Rev. 62, 129–142.
Pitcairn, I.K., Craw, D., Teagle, D.A.H., 2015. Metabasalts as sources of metals in orogenic gold deposits. Mineral. Depos. 50, 373–390.
Renock, D., Becker, U., 2011. A first principles study of coupled substitution in galena. Ore Geol. Rev. 42, 71–83.
Rice, C.M., Mark, D.F., Selby, D., Hill, N.J., 2012. Dating vein-hosted Au deposits in the Caledonides of N. Britain. Trans. Inst. Min. Metall. (Section B. Appl. Earth. Sci.) 121, 199–200.
Rudnick, R.L., Gao, S., 2014. Composition of the Continental Crust. Elsevier, pp. 1–51 2nd edition, Volume 4, Chapter 1 in Treatise on Geochemistry.
Robert, F., 2001. Syenite-associated disseminated gold deposits of the Abitibi greenstone belt Canada. Miner. Depos. 36, 503–516.
Robinson, B.W., Kusakabe, M., 1975. Quantitative preparation of sulfur dioxide, for $^{34}S/^{32}S$ analyses, from sulfides by combustion with cuprous oxide. Anal. Chem. 47, 1179–1181.
Science and Technology Committee, House of Commons, 2011. Strategically important metals. HC 726, The Stationery Office Limited, London.
Scotgold Resources Limited, 2015. Cononish gold project study update and JORC 2012 ore reserve estimate http://www.asx.com.au/asxpdf/20150526/pdf/42yt26kn3xqj6x.pdf.
Sillitoe, R.H., Thompson, J.F.H., 1998. Intrusion-related vein gold deposits: types, tectono-magmatic settings and difficulties of distinction from orogenic gold deposits. Res. Geol. 48, 237–250.
Spence-Jones, C., 2013. Metallurgical investigation of ore at Cononish Gold Mine, Scotland. Unpub. MGeol thesis. University of Leicester.
Stephenson, D., Mendum, J.R., Fettes, D.J., Leslie, A.G., 2013. The dalradian rocks of Scotland: an introduction. Proc. Geol. Ass. 124, 3–82.
Stüwe, K., 1998. Tectonic constraints on the timing relationships of metamorphism, fluid production and gold-bearing quartz vein emplacement. Ore Geol. Rev. 13, 219–228.
Tanner, P.W.G., 2012. The giant quartz-breccia veins of the Tyndrum-Dalmally area, Grampian Highlands, Scotland: their geometry, origin and relationship to the Cononish gold-silver deposit. Earth Environ. Sci. Trans. Roy. Soc. Edinburgh 103, 51–76.
Tanner, P.W.G., 2014. Structural controls and origin of gold–silver mineralization in the Grampian terrane of Scotland and Ireland. Geol. Mag. 151, 1072–1094.
Tanner, P.W.G., Thomas, P.R., 2010. Major nappe–like D2 folds in the Dalradian rocks of the Beinn Udlaidh area, Central Highlands, Scotland. Earth and Environ. Sci. Trans. Roy. Soc. Edinburgh 100, 371–389.
Thompson, J.F.H., Sillitoe, R.H., Baker, T., Lang, J.R., Mortensen, J.K., 1999. Intrusion-related gold deposits associated with tungsten-tin provinces. Miner. Depos. 34, 323–334.
Treagus, J.E., Pattrick, R.A.D., Curtis, S.F., 1999. Movement and mineralization in the Tyndrum fault zone, Scotland and its regional significance. J. Geol. Soc. 156, 591–604.
Treloar, P.J., Lawrence, D.M., Senghor, D., Boyce, A., Harbidge, P., 2015. The Massawa gold deposit, Eastern Senegal, West Africa: an orogenic gold deposit sourced from magmatically derived fluids? In: Jenkin, G.R.T., Lusty, P.A.J., McDonald, I., Smith, M.P., Boyce, A.J., Wilkinson, J.J. (Eds.), Ore Deposits in an Evolving Earth. Geol. Soc. Lond. Spec. Publ., pp. 135–160.
Wedepohl, K.H., 1995. The composition of the continental-crust. Geochim. Cosmochim. Acta 59, 1217–1232.
Woodhouse, M., Goodrich, A., Margolis, R., James, T., Dhere, R., Gessert, T., Barnes, T., Eggert, R., Albin, D., 2013. Perspectives on the pathways for cadmium telluride photovoltaic module manufacturers to address expected increases in the price for tellurium. Solar Energy Mat. Solar Cells 115, 199–212.
Wyman, D.A., Cassidy, K.F., Hollings, P., 2016. Orogenic gold and the mineral systems approach: Resolving fact, fiction and fantasy. Ore Geol. Rev. 78, 322–335.
Yoo, B.C., Lee, H.K., White, N.C., 2010. Mineralogical, fluid inclusion, and stable isotope constraints on mechanisms of ore deposition at the Samgwang mine (Republic of Korea) – a mesothermal, vein hosted gold-silver deposit. Mineral. Depos. 45, 161–187.